

Synthesis and magnetic properties of large-area ferromagnetic cylindrical nanoshell and nanocup arrays

Z. Wang, G. Shimon, X. Liu, C. V. Thompson, C. A. Ross, W. K. Choi, and A. O. Adeyeye

Citation: *Journal of Applied Physics* **113**, 214301 (2013); doi: 10.1063/1.4808103

View online: <http://dx.doi.org/10.1063/1.4808103>

View Table of Contents: <http://scitation.aip.org/content/aip/journal/jap/113/21?ver=pdfcov>

Published by the AIP Publishing

Articles you may be interested in

[Magnetic properties of square Py nanowires: Irradiation dose and geometry dependence](#)

J. Appl. Phys. **117**, 173903 (2015); 10.1063/1.4919839

[Switching behavior of lithographically fabricated nanomagnets for logic applications](#)

J. Appl. Phys. **111**, 07B911 (2012); 10.1063/1.3676220

[Influence of dot size and annealing on the magnetic properties of large-area L10-FePt nanopatterns](#)

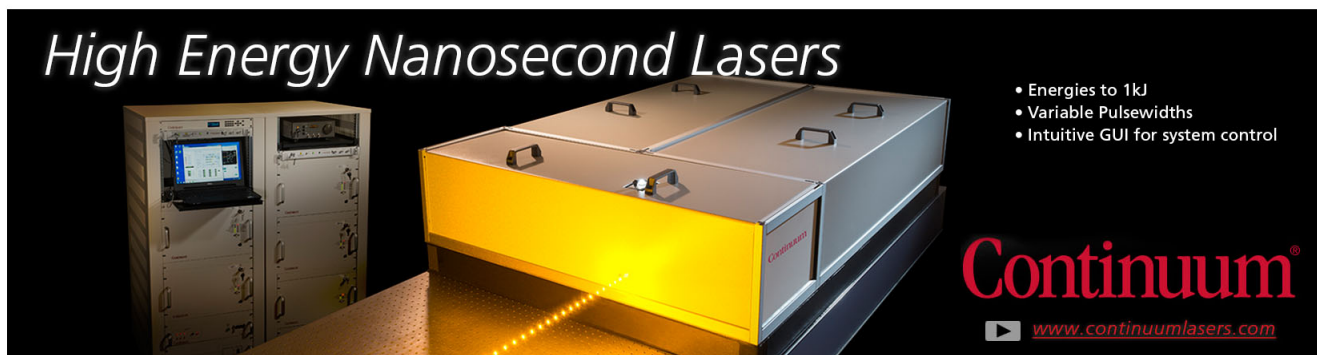
J. Appl. Phys. **110**, 073908 (2011); 10.1063/1.3646550

[Torque studies of large-area Co arrays fabricated by etched nanosphere lithography](#)

J. Appl. Phys. **97**, 10J503 (2005); 10.1063/1.1849665

[Shape effect on magnetization reversal in chains of interacting ferromagnetic elements](#)

Appl. Phys. Lett. **82**, 3716 (2003); 10.1063/1.1577808

An advertisement for Continuum High Energy Nanosecond Lasers. The image shows a large, industrial-grade laser system with a prominent yellow glow from the laser output. To the left, there is a control console with a monitor and various buttons. The background is dark, making the laser and its components stand out. The text 'High Energy Nanosecond Lasers' is written in a white, serif font at the top left. On the right, there is a list of features: 'Energies to 1kJ', 'Variable Pulsewidths', and 'Intuitive GUI for system control'. The Continuum logo is in red at the bottom right, with the website address 'www.continuumlasers.com' below it.

High Energy Nanosecond Lasers

- Energies to 1kJ
- Variable Pulsewidths
- Intuitive GUI for system control

Continuum[®]

www.continuumlasers.com

Synthesis and magnetic properties of large-area ferromagnetic cylindrical nanoshell and nanocup arrays

Z. Wang,¹ G. Shimon,¹ X. Liu,^{1,2,3} C. V. Thompson,^{1,4} C. A. Ross,^{1,4} W. K. Choi,^{1,5,a)} and A. O. Adeyeye^{1,5,a)}

¹Advanced Materials for Micro- and Nano-Systems Program, Singapore-MIT Alliance, National University of Singapore, Singapore 117576, Singapore

²Department of Chemistry, National University of Singapore, Singapore 117543, Singapore

³Institute of Materials Research and Engineering, Singapore 117602, Singapore

⁴Department of Materials Science and Engineering, Massachusetts Institute of Technology, Cambridge, Massachusetts 02139, USA

⁵Department of Electrical and Computer Engineering, National University of Singapore, Singapore 117576, Singapore

(Received 9 March 2013; accepted 14 May 2013; published online 4 June 2013)

Large-area arrays of magnetic Ni₈₀Fe₂₀ cylindrical nanoshells, nanocups, and perforated nanocups were synthesized using oblique deposition into topographical templates patterned using laser interference lithography. The geometry of the template and the tilt angle of the sample during deposition provide versatile control over the final geometry and dimension of nanostructures with thickness below 10 nm. Decreasing shell thickness led to a magnetization switching path between onion (bidomain) and reverse onion states, bypassing the vortex (flux-closed) state. The variation of magnetization reversal processes with geometry was characterized using vibrating sample magnetometry, and the results were in good agreement with micromagnetic simulations.

© 2013 AIP Publishing LLC. [<http://dx.doi.org/10.1063/1.4808103>]

I. INTRODUCTION

Ferromagnetic nanorings and nanotubes have attracted extensive research interest both for fundamental studies of magnetism in confined geometries^{1–5} and for their relevance to devices for data storage,^{6,7} spin valves,⁸ and sensors.^{9,10} Nanoscale magnetic ring arrays have been fabricated using various processes including optical lithography,² electron beam lithography,¹¹ nanosphere lithography,^{12,13} anodic alumina templating,¹⁴ and block copolymer templating.^{15,16} Magnetic nanotube arrays have been fabricated by electrochemical deposition, atomic layer deposition, shadowed evaporation over an anodized alumina template,^{17–20} or ion milling of a conformal ferromagnetic thin film deposited on resist pillars patterned by electron beam lithography.²¹

Most work on ferromagnetic nanorings has focused on flat thin film rings in which the ring height or thickness (h) is significantly smaller than the ring width (w) and diameter (d). In the absence of strong magnetocrystalline or magnetoelastic anisotropies, these rings have in-plane magnetization over a range of materials and h , w , and d dimensions. They exhibit an onion (O) - vortex (V) - reverse onion (RO) switching path during magnetization reversal under an in-plane field.^{2,22} In the V-state, the magnetization forms a flux closure and is oriented circumferentially around the ring, clockwise, or counterclockwise. In the O or RO-state, there are two semicircular magnetic domains separated by a head-to-head and a tail-to-tail domain wall (DW) at opposite sides of the ring. A vortex-type domain wall (VW) forms in order to minimize the magnetostatic energy in nanorings with larger h and w . For rings with

smaller h and w , transverse walls (TW) are promoted because they have lower exchange energies,^{23–25} although in very thin rings with h below 4 nm, VWs may be favoured due to structural defects.²⁴ Stray fields are present around the DWs,^{2,25,26} with greater in-plane magnitude for TWs, which can lead to magnetostatic interactions between adjacent rings.²⁷

In contrast, nanotubes represent a ring geometry which has $h \gg w$. They exhibit coherent or curling modes of magnetization switching depending on dimensions and material.^{28–30} Long nanotubes with high aspect ratios tend to have an easy axis along the tube.^{4,20,30} For shorter NiFe nanotubes with an outer d of 300 nm, w of 20 nm, and h of 600 nm, the hysteresis loop for an in-plane field exhibited multi-step switching. Simulations show that the magnetic moments reversed incoherently along the cylinder, and VWs were present.²¹

In this article, we present a fabrication method for making large-area ordered arrays of Ni₈₀Fe₂₀ cylindrical nanoshells using a template patterned by laser interference lithography and reactive ion etching (RIE), coated using oblique-incidence evaporation. Nanoshells are defined as short nanotubes or tall nanorings, in which the height is a few times greater than the width. Using this method, structures with a sub-10 nm shell width were achieved, and their switching process was characterized as a function of the width w . This method was also used to produce nanocups and perforated nanocups, which are nanotubes with complete or ring-shaped circular bases, and their reversal processes were compared with those of the nanotubes.

II. EXPERIMENT

Figure 1 depicts the fabrication process and the corresponding SEM micrographs after each step. A

^{a)}Authors to whom correspondence should be addressed. Electronic addresses: elechoi@nus.edu.sg and eleaao@nus.edu.sg

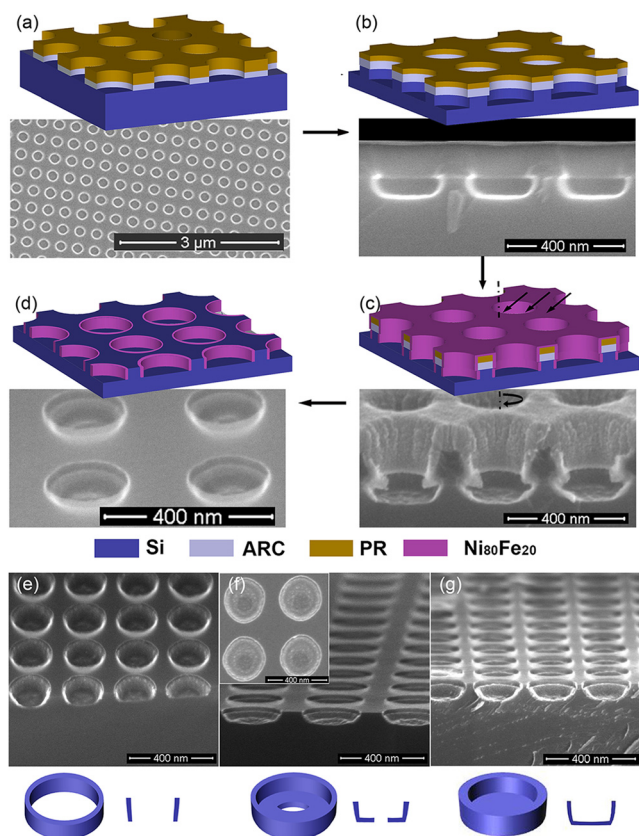


FIG. 1. Schematics of the fabrication process and corresponding SEM micrographs after each step: (a) interference lithography, (b) reactive ion etching, (c) NiFe electron beam evaporation, and (d) lift off. (e)–(g) are SEM micrographs and schematics of the final structure for cylindrical nanoshells, perforated nanocups, or nanocups, respectively, and the inset in (f) is a top view of the perforated nanocups.

developer-soluble anti-reflective coating (ARC) layer and negative photoresist were spin-coated on a silicon wafer. Arrays of holes were patterned in the resist stack using interference lithography with a Lloyd's mirror configuration and a 325 nm helium–cadmium laser (Figure 1(a)). The diameter and period of holes were determined by the exposure dose and interference angle. The pattern was then transferred into the silicon substrate using reactive ion etching (RIE), as shown in Figure 1(b). The under-cut resist profile at the sidewall after etching assisted the final lift-off process of the magnetic metal. Subsequently, NiFe (Ni 80%, Fe 20%) was deposited on the sidewall of the holes by an angular deposition process¹⁵ in an electron beam evaporator. The rotating substrate was tilted at an angle with respect to the flux during the evaporation process, as shown in Figure 1(c). Figure 1(d) depicts the final lift-off process which led to arrays of NiFe cylindrical nanoshells.

This method is highly versatile for controlling the dimensions and geometry of the nanostructures. The period of the arrays was varied from 250 nm to 400 nm, and the outer diameter of the shell was varied from 180 nm to 300 nm. The w varied from 25 nm to sub-10 nm, and h was varied from 30 nm to 50 nm. Depending on the template geometry and tilt angle during NiFe deposition, the final nanostructure was a cylindrical nanoshell, a perforated

nanocup, or a nanocup with a continuous base, as shown in Figures 1(e)–1(g), respectively.

The in-plane magnetization reversal processes were characterized using a Vibrating Sample Magnetometer (VSM) with a field range of ± 3 kOe. Micromagnetic simulations for a single nanostructure were performed using the Object Oriented MicroMagnetic Framework (OOMMF) program from NIST.³¹ To simplify the calculation, the nanostructures were assumed to have walls of uniform thickness. The dimensions used in the simulations were extracted from SEM micrographs of the nanostructures. The following parameters were used for NiFe: saturation magnetization = 860 emu/cm^3 , exchange constant $A = 1.3 \times 10^{-6} \text{ erg/cm}$, and the Gilbert damping parameter was set at 0.5 for rapid convergence. The magnetocrystalline anisotropy was treated as negligible when compared with the shape-induced anisotropy of the nanostructures. The cell size used was $2 \times 2 \times 2 \text{ nm}^3$ for the nanoshell and $4 \times 4 \times 5 \text{ nm}^3$ for the nanocup.

III. RESULTS AND DISCUSSION

A. Cylindrical NiFe nanoshells

1. Effect of shell width

There was a good qualitative agreement between experiments and simulations for the effect of w on magnetization switching of nanoshells. Figure 2 shows the measured and simulated in-plane M-H loops for nanoshells with w of 8 nm (Figures 2(a) and 2(b)), 18 nm (Figures 2(d) and 2(e)), and 25 nm (Figures 2(g) and 2(h)). Figures 2(c), 2(f), and 2(i) are the simulated magnetic configurations at designated fields in Figures 2(b), 2(e), and 2(h). These nanoshells had an average d of 196 nm with a standard deviation of 5.7 nm. The height was approximately 40 nm, and period was 250 nm.

Two-step switching was observed for thicker nanoshells with $w = 18$ nm and 25 nm. Figures 2(f) and 2(i) show the magnetization reversal process which corresponded to O-V-RO transitions similar to those of thin film ferromagnetic nanorings,^{2,6} despite the greater height/width ratio of the nanoshells compared to rings. In the O-V transition (e1-e2 and h1-h2), simulations showed that the head-head and tail-tail DWs depinned, moved towards each other, and annihilated to form a flux closure V-state. At higher field, the V-RO transition occurred (e3-e4 and h3-h4) when a reverse domain nucleated and reversed the magnetization in half of the shell to form the RO-state.

In comparison, the nanoshell array with w of 8 nm showed a single-step switching process at b2-b3 corresponding to the O-RO transition with a much narrower hysteresis loop. No V-state stability range was observed in the experiments or simulations. Similar single-step switching has been reported in a theoretical study for Fe nanoshells with $d = 80$ nm, $w = 8$ nm, $h > 120$ nm (Ref. 32) and in experimental studies of long nanotubes.^{20,28,30}

The competition of exchange, demagnetization, and Zeeman energies associated with the ferromagnetic structure under an external magnetic field determines its magnetization reversal process. For nanoshells with w of 18 nm and 25 nm, exchange and demagnetization energies dropped at

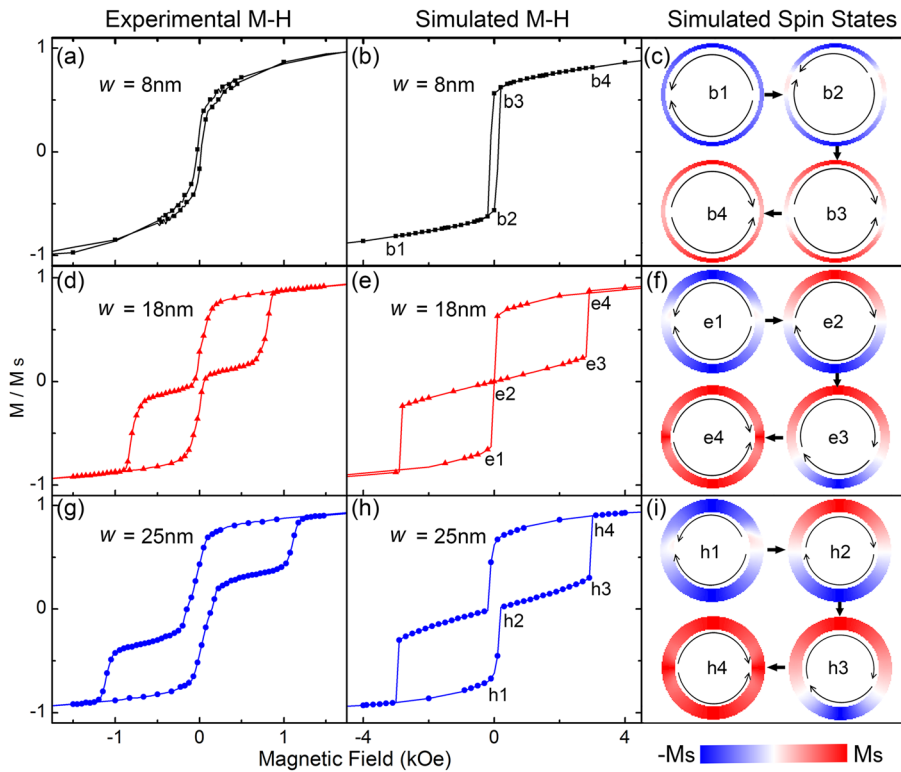


FIG. 2. Experimental M-H loops (a), (d), (g), simulated M-H loops (b), (e), (h), and simulated magnetic configurations (c), (f), (i) for w equal to (a), (b), (c) 8 nm, (d), (e), (f) 18 nm, and (g), (h), (i) 25 nm. The color code in (c), (f), (i) represents the horizontal component of the magnetization.

remnance and energy valleys appeared as the V-state formed. For nanoshells with w of 8 nm, there were no such energy valleys and the V-state was absent (Figure S1 in supplementary material).³³

2. Spin configurations at domain walls

The magnetic configuration of the DWs in nanoshells and the nearest-neighbor magnetostatic interactions are important in understanding the switching behavior of the arrays. DW phase diagrams for nanorings in the onion state with varying h and w have been plotted for NiFe (Ref. 24) and Co (Ref. 25), showing that a TW is expected in nanorings with smaller h and w . However, the nanoshells have $h/w > 1$, and it is therefore likely that the transverse component of the TW will be oriented along the out-of-plane h direction, not radially along w . Figures 3(b) and 3(c) show the y - z plane views of the simulated DW in a nanoshell with w of 8 nm at cross

sections indicated in Figure 3(a), confirming that the moments in the center of the TW point out of plane. A similar DW structure was reported in a Monte Carlo simulation for nanorings with ring $d = 70$ nm, $w = 7$ nm, and $h = 10$ nm.³⁴ The cylindrical nanoshell can thus be viewed as a rolled-up thin film strip containing two TWs.³⁵ This DW configuration yielded a lower in-plane stray field but a higher out-of-plane stray field as shown in Figures 3(d) and 3(e). In nanoshells with w of 18 nm and 25 nm, the moments in the center of TW still pointed in the h direction. However, the component in the x - y plane increased.

Figure 3(d) shows the in-plane magnitude ($H_x^2 + H_y^2$)^{0.5} of the simulated stray field around a DW in a NiFe ring with $d = 200$ nm, $w = 8$ nm, and $h = 40$ nm. The stray field 50 nm away from the DW in the $-x$ direction was calculated as 164 Oe. Such a field is significant compared to the switching field. It would lead to stabilization of parallel O-states and correlated reversal of the nanoshells.

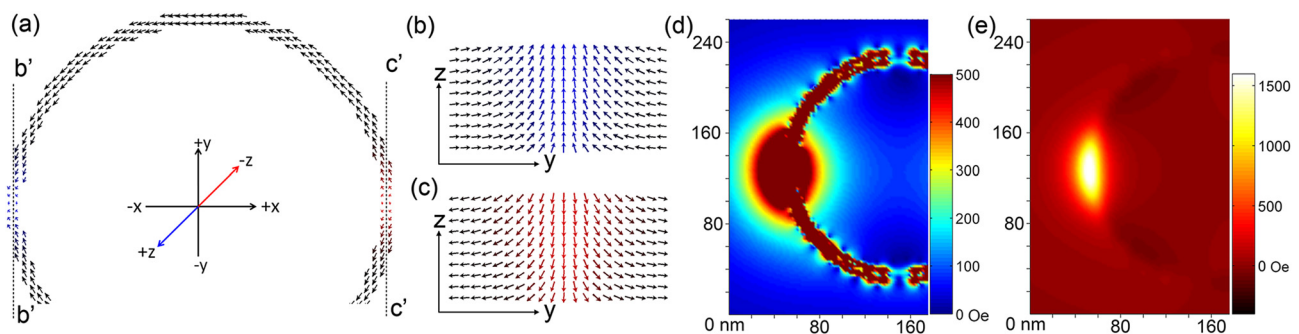


FIG. 3. Spin configuration of a nanoshell with w of 8 nm, d of 200 nm, and h of 40 nm (a) top view, (b) y - z plane view at cross section b'-b', (c) y - z plane view at cross section c'-c'. (d) Calculated in-plane root mean square magnitude in the x - y plane of the stray field around a DW at half of the shell height. (e) Calculated out-of-plane stray field around a DW at a height of 10 nm above the shell.

3. Effect of structural asymmetry

The effect of structural asymmetry was also investigated using micromagnetic simulations (Figure S2 in supplementary material³³). Reversal of a nanoshell with $d=200$ nm, $h=40$ nm, but inhomogeneous w varying from 6 nm to 10 nm were simulated. The asymmetric nanoshell exhibited two-step switching via O-V-RO states³³ compared to the O-RO switching in a symmetric nanoshell of the same size. The narrower region of the shell acted as a DW pinning site in the O-state, breaking the symmetry between the two walls. DW pinning due to structural asymmetry or defects facilitates the formation of a V-state with a specific chirality.^{36–38}

B. Perforated nanocup and nanocup

The perforated nanocup exhibited a four-step switching process, as shown in Figures 4(a) and 4(b). The structure can be considered as having two regions: a top cylindrical shell and a bottom thin film ring. Figures 4(e)–4(i) show the magnetization evolution of the shell and ring regions. The

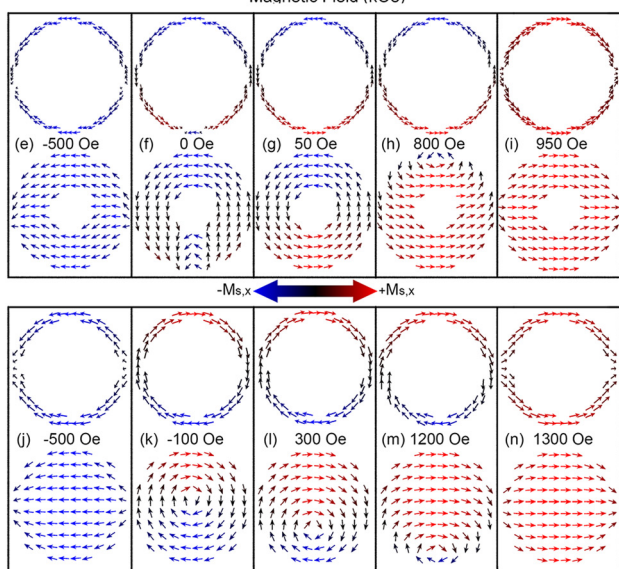
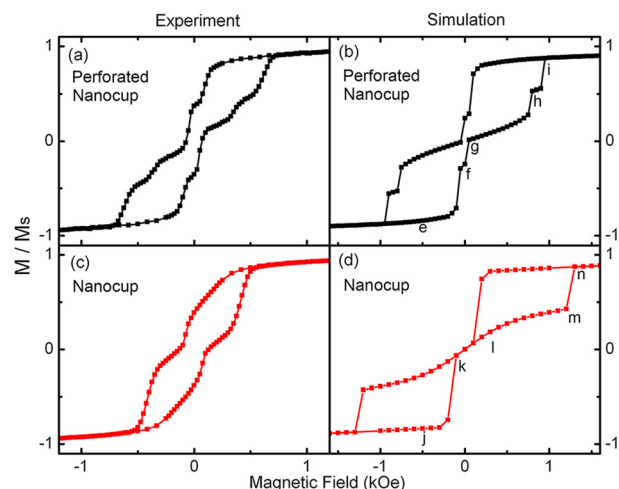


FIG. 4. Experimental M-H loops and simulated M-H loops for the perforated nanocup (a), (b) and the nanocup (c), (d). (e)–(i) and (j)–(n) show the simulated magnetization states of the shell and ring region for a perforated nanocup and for a nanocup, respectively, at the designated fields. The color code in (e)–(n) represents the horizontal component of the magnetization.

reversal started with an overall O-state when relaxed from in-plane saturation (Figure 4(e)). At remanence (Figure 4(f)), the two DWs depinned but did not annihilate to form a vortex state. Instead, the two DWs formed a 360° DW in the shell region, while a TW was formed in the ring region. The junction between ring and shell regions created a barrier for magnetization rotation and inhibited DW annihilation. As the field increased, V-states formed in both ring and shell regions (Figure 4(g)). At 800 Oe (Figure 4(h)), the shell region retained a V-state, but two domains formed in the ring region, and a small part of the ring at the edge had its magnetization anti-parallel to the applied field due to exchange coupling with the shell region. The two domains in the ring were separated by a VW. When the field was increased further in the $+x$ direction, a RO state formed throughout the structure (Figure 4(i)).

In contrast, the nanocup structure showed a two-step switching, as shown in Figures 4(c) and 4(d). The structure can be considered as two regions: a top cylindrical shell and a bottom thin film circular disk. After relaxation from in-plane saturation, the shell region was in an O-state, while in the disk region the moments aligned along the $-x$ direction except the edge part (Figure 4(j)). At -100 Oe, the shell switched into a V-state, while a vortex also nucleated in the disk (Figure 4(k)). As the field increased along the $+x$ direction, the two DWs in the shell depinned and moved toward each other. At the same time, the vortex core in the disk moved toward one side of the disk, and more of the moment of the disk aligned with the external field (Figures 4(l) and 4(m)). Finally, the two DWs in the top shell region annihilated each other, while the vortex in the bottom disk annihilated at the edge (Figure 4(n)).

IV. CONCLUSION

In conclusion, a fabrication method for making ordered arrays of cylindrical nanoshell, perforated nanocup, and nanocup structures has been demonstrated. Combining interference lithography and angular deposition, the maskless and parallel nature of this nanofabrication method enables high-throughput, large-area fabrication of nanostructure arrays. The process is versatile, enabling fabrication of different geometries with controlled dimensions. By varying the shell thickness w , the magnetic reversal process of cylindrical NiFe nanoshells was markedly modified. As w decreased to 8 nm, nanoshells showed an O-RO switching without going through a V-state. A combination of thin w and high height/width (h/w) ratio led to transverse domain walls with an out-of-plane orientation in the O-state. In NiFe nanocup arrays, a two-step O-V-RO switching was observed with correlated switching of the top shell and the bottom disk regions. In comparison, the perforated nanocup arrays showed a four-step switching process as the top shell and bottom thin film ring regions reversed at different fields. This method is not limited to fabrication of ferromagnetic nanostructures but may also be used to fabricate ordered nanoshell/nanocup arrays of other materials for a range of potential applications in plasmonics, photonics, and optoelectronics, such as

surface plasmon resonance based biosensors³⁹ and nanoscale optical sensors.⁴⁰

ACKNOWLEDGMENTS

The authors would like to acknowledge the support from Singapore-MIT Alliance and Institute of Materials Research and Engineering, Singapore.

- ¹G. D. Chaves-O'Flynn, A. D. Kent, and D. L. Stein, *Phys. Rev. B* **79**, 184421 (2009).
- ²G. Shimon, A. O. Adeyeye, and C. A. Ross, *J. Appl. Phys.* **111**, 013909 (2012).
- ³M. D. Mascaro, H. S. Korner, C. Nam, B. G. Ng, and C. A. Ross, *Appl. Phys. Lett.* **98**, 252506 (2011).
- ⁴Z. K. Wang, H. S. Lim, H. Y. Liu, S. C. Ng, M. H. Kuok, L. L. Tay, D. J. Lockwood, M. G. Cottam, K. L. Hobbs, P. R. Larson, J. C. Keay, G. D. Lian, and M. B. Johnson, *Phys. Rev. Lett.* **94**, 137208 (2005).
- ⁵J. Lee, D. Suess, T. Schrefl, K. H. Oh, and J. Fidler, *J. Magn. Magn. Mater.* **310**, 2445 (2007).
- ⁶J. G. Zhu, Y. Zheng, and G. A. Prinz, *J. Appl. Phys.* **87**, 6668 (2000).
- ⁷X. F. Han, Z. C. Wen, and H. X. Wei, *J. Appl. Phys.* **103**, 07E933 (2008).
- ⁸X. M. Liu, S. Jain, and A. O. Adeyeye, *IEEE Trans. Magn.* **47**, 2628 (2011).
- ⁹X. Hu, J. C. Yu, J. Gong, Q. Li, and G. Li, *Adv. Mater.* **19**, 2324 (2007).
- ¹⁰M. Y. Liao, C. C. Huang, M. C. Chang, S. F. Lin, T. Y. Liu, C. H. Su, C. S. Yeh, and H. P. Lin, *J. Mater. Chem.* **21**, 7974 (2011).
- ¹¹L. J. Heyderman, M. Kläui, B. Nöhammer, C. A. F. Vaz, J. A. C. Bland, and C. David, *Microelectron. Eng.* **73–74**, 780 (2004).
- ¹²F. Q. Zhu, D. Fan, X. Zhu, J. G. Zhu, R. C. Cammarata, and C. L. Chien, *Adv. Mater.* **16**, 2155 (2004).
- ¹³M. Bayati, P. Patoka, M. Giersig, and E. R. Savinova, *Langmuir* **26**, 3549 (2010).
- ¹⁴Y. L. Li, S. L. Tang, W. B. Xia, L. Y. Chen, Y. Wang, T. Tang, and Y. W. Du, *Appl. Phys. Lett.* **100**, 183101 (2012).
- ¹⁵D. K. Singh, R. V. Krotkov, H. Xiang, T. Xu, T. P. Russell, and M. T. Tuominen, *Nanotechnology* **19**, 245305 (2008).
- ¹⁶D. K. Singh, R. Krotkov, and M. T. Tuominen, *Phys. Rev. B* **79**, 184409 (2009).
- ¹⁷J. C. Hulthén and C. R. Martin, *J. Mater. Chem.* **7**, 1075 (1997).
- ¹⁸K. L. Hobbs, P. R. Larson, G. D. Lian, J. C. Keay, and M. B. Johnson, *Nano Lett.* **4**, 167 (2004).
- ¹⁹M. D. Dickey, E. A. Weiss, E. J. Smythe, R. C. Chiechi, F. Capasso, and G. M. Whitesides, *ACS Nano* **2**, 800 (2008).
- ²⁰M. Daub, M. Knez, U. Goesele, and K. Nielsch, *J. Appl. Phys.* **101**, 09J111 (2007).
- ²¹Y. C. Huang, C. Y. Kuo, J. H. Shyu, C. M. Lee, L. Horng, and J. C. Wu, *J. Vac. Sci. Technol. B* **30**, 06FF07 (2012).
- ²²J. Rothman, M. Kläui, L. Lopez-Diaz, C. A. F. Vaz, A. Bleloch, J. A. C. Bland, Z. Cui, and R. Speaks, *Phys. Rev. Lett.* **86**, 1098 (2001).
- ²³C. A. F. Vaz, T. J. Hayward, J. Llandro, F. Schackert, D. Morecroft, J. A. C. Bland, M. Kläui, M. Laufenberg, D. Backes, U. Rüdiger, F. J. Castaño, C. A. Ross, L. J. Heyderman, F. Nolting, A. Locatelli, G. Faini, S. Cherifi, and W. Wernsdorfer, *J. Phys.: Condens. Matter* **19**, 255207 (2007).
- ²⁴M. Laufenberg, D. Backes, W. Bührer, D. Bedau, M. Kläui, U. Rüdiger, C. A. F. Vaz, J. A. C. Bland, L. J. Heyderman, F. Nolting, S. Cherifi, A. Locatelli, R. Belkhou, S. Heun, and E. Bauer, *Appl. Phys. Lett.* **88**, 052507 (2006).
- ²⁵M. Kläui, C. A. F. Vaz, J. A. C. Bland, L. J. Heyderman, F. Nolting, A. Pavlovskaya, E. Bauer, S. Cherifi, S. Heun, and A. Locatelli, *Appl. Phys. Lett.* **85**, 5637 (2004).
- ²⁶S. P. Li, D. Peyrade, M. Natali, A. Lebib, Y. Chen, U. Ebels, L. D. Buda, and K. Ounadjela, *Phys. Rev. Lett.* **86**, 1102 (2001).
- ²⁷C. Nam, M. D. Mascaro, and C. A. Ross, *Appl. Phys. Lett.* **97**, 012505 (2010).
- ²⁸X. F. Han, S. Shamaila, R. Sharif, J. Y. Chen, H. R. Liu, and D. P. Liu, *Adv. Mater.* **21**, 4619 (2009).
- ²⁹C. R. Chang, C. M. Lee, and J. S. Yang, *Phys. Rev. B* **50**, 6461 (1994).
- ³⁰D. D. Li, R. S. Thompson, G. Bergmann, and J. G. Lu, *Adv. Mater.* **20**, 4575 (2008).
- ³¹M. J. Donahue and D. G. Porter, OOMMF User's Guide, Version 1.0, Interagency Report NISTIR 6376, National Institute of Standards and Technology, Gaithersburg, September 2009.
- ³²J. J. Torres-Heredia, F. López-Urías, and E. Muñoz-Sandoval, *J. Magn. Magn. Mater.* **294**, e1 (2005).
- ³³See supplementary material at <http://dx.doi.org/10.1063/1.4808103> for volumetric exchange, demagnetization, and Zeeman energies vs. external field for nanoshells with width of 8 nm and 25 nm and for simulated reversal of asymmetric nanoshells.
- ³⁴W. Zhang and S. Haas, *Phys. Rev. B* **81**, 064433 (2010).
- ³⁵R. D. McMichael and M. J. Donahue, *IEEE Trans. Magn.* **33**, 4167 (1997).
- ³⁶F. Q. Zhu, G. W. Chern, O. Tchernyshyov, X. C. Zhu, J. G. Zhu, and C. L. Chien, *Phys. Rev. Lett.* **96**, 027205 (2006).
- ³⁷X. H. Wang, W. K. Peng, and W. S. Lew, *J. Appl. Phys.* **106**, 043905 (2009).
- ³⁸F. Giesen, J. Podbielski, B. Botters, and D. Grundler, *Phys. Rev. B* **75**, 184428 (2007).
- ³⁹E. M. Larsson, J. Alegret, M. Käll, and D. S. Sutherland, *Nano Lett.* **7**, 1256 (2007).
- ⁴⁰Y. B. Zheng, S. J. Wang, A. C. H. Huan, and Y. H. Wang, *J. Non-Cryst. Solids* **352**, 2532 (2006).